Modelling the influence of soil properties on performance and bioremediation ability of a pile of soil microbial fuel cells

Elisa Casula[1 †], Bongkyu Kim[2,3 †], Henry Chesson[2], Mirella Di Lorenzo[2,3*], Michele Mascia[1*]

[1]*Dipartimento di Ingegneria Meccanica, Chimica e dei Materiali, Università degli Studi di Cagliari, Via Marengo 2, Cagliari, 09123, Italy*

[2]*Department of Chemical Engineering, University of Bath, BA2 7AY, Bath, UK*

[3]*Centre for Biosensors, Bioelectronics and Biodevices, University of Bath, BA2 7AY, Bath, UK*

[†]*These authors contributed equally to the manuscript*

**corresponding authors:*

m.di.lorenzo@bath.ac.uk

michele.mascia@unica.it

Abstract

Worldwide, intense industrial and agricultural activities pose serious issues of land contamination. Soil microbial fuel cells (SMFCs) have great potential as a low-cost, and self-powered solution to soil bioremediation, compatible with operations in remote areas. In this study, we propose a novel tubular SMFC design, in which a ceramic tube acts as the separator between the air-cathode and the anode, while providing structural support. No oxygen reduction reaction catalyst is used, and to reach depth, several SMFC units are piled together.

To assess the effect of both the system design and soil properties on performance, a mathematical model is proposed, which accounts for chemical and (bio)electrochemical reactions, as well as for charge conservation and transport phenomena, and is calibrated with experimental data. The information generated provides useful indications on optimal design and operational conditions for SMFCs and a guide to effective scale-up strategies for their use in bioremediation.

Keywords: Soil microbial fuel cell; Bioremediation; Modelling; Hexachlorobenzene

List of Symbols

Symbol	Description	Units
a_j	Specific area of electrodes	$17{,}700\ m^{-1}$
C_i	Concentration of i-th species	$mol\ m^{-3}$
C_{W_c}	Threshold water content	$mol\ m^{-3}$
$\mathcal{D}_i$	Free diffusivity of ith species in water	$m^2\ s^{-1}$
$\mathcal{D}_{i,j}$	Effective diffusivity ith species in the jth domain	$m^2\ s^{-1}$
E_j^0	Electrode standard potential	V
h_W	Coefficient of water evaporation	$m\ s^{-1}$
F	Faraday's Constant	$96{,}485\ C\ mol^{-1}$
I	Volumetric current density	$A\ m^{-3}$
k_k	Specific rate of kth reaction	$mol\ m^{-3}\ s^{-1}$
k_d	Inactivation constant for biofilm	d^{-1}
K	Half-saturation constant	$mol\ m^{-3}$
R	Universal constant of gases	$8.314\ J\ mol\ K^{-1}$
T	Temperature	K
V_j	Electric potential in the j-th domain	V
z_k	Number of electrons in kth reaction	-

Subscripts		Greek letters		
M_S	Suspended microorganisms	ε	Porosity of the j-th domain	-
M_A	Adhered microorganisms	η	Electrode over-potential	V
W	Water	ν	Stoichiometric coefficient	-
W_{Vap}	Water vapour	σ	Electric Conductivity	$S\ m^{-1}$
OM	Natural Organic Matter			
OP	Organic Pollutant			

1. Introduction

Agricultural and industrial intensification, consequent to population growth and rapid urbanisation, are a growing source of organic (i.e herbicides, pesticides, petroleum hydrocarbons) and inorganic (i.e. metals, metalloids) contamination in soils, threatening ecosystems and human health [1]. Pesticides are amongst the most widespread pollutants in the environment, causing serious deteriorations of soil quality and the environment [2]. Some organic pesticides can persist in the environment for long periods of time. Along with their metabolites, these compounds can accumulate in the soil at unacceptable high levels, which can be extremely toxic and can bio magnify in the food chain [3]. Although the use of these persistent pesticides has been globally banned by the United Nations Environment Programme Governing Council, to prevent or minimise further release into the environment, the development of effective technologies to remediate contaminated soil is still of critical importance. In this context, bioremediation strategies represent a cost-effective and environmentally friendly alternative to traditional physical-chemical treatments [4]. Strategies like bioaugmentation, phytoremediation, and biostimulation allows in situ stabilization and/or extraction of contaminants [5]. The combination of these approaches can help address the limitations of each and is highly recommended to address soil co-contamination by different pollutants [4]. Nonetheless, these bioremediation strategies are limited by low oxygen levels in soil and slow activity of microbial community, leading to unpredictable performance in the field [6].

Microbial electrochemical systems, such as Soil Microbial Fuel Cells (SMFCs), offer the attractive benefit of integrating together microbial and electrochemical processes for a faster and more effective treatment than other bioremediation strategies [7]. In SMFCs, the anode is exposed to the soil, while the cathode is exposed to air [8]. The soil acts then as the

electrolyte and the source of organic and electroactive microorganisms [9]. SMFCs are intended for direct in-field installation and remediation; at the anode of SMFCs, organic contaminants are oxidised via the action of electroactive bacteria in anaerobic conditions, while useful electrical energy is generated, which could be used for example to power a remote sensor [7]. SMFCs have successfully demonstrated to remove organic pollutants in soil, such as petroleum hydrocarbons [10], diesel [11], phenols [12], and pesticides [7, 13-15].

Both flat and tubular geometries have been proposed for SMFCs. In flat geometries, the anode is buried into the soil while the cathode, exposed to air, is placed onto the soil surface [16]. While being very simple and low-cost, this geometry challenges practical bioremediation applications in the field. The optimal electrode distance in this configuration would in fact limit the depth at which the soil can be treated. Enhanced depth could instead be reached with a tubular geometry. In this geometry, the two electrodes are arranged in concentric layers, with the anode directly exposed to the soil in the outer layer, and the cathode in the hollow inner layer exposed to air [17, 18]. Contrary to the flat geometry, where the soil itself separates the two electrodes, the tubular geometry needs a separator, which adds complexity in the design and may increase both the internal resistance and the cost of the overall system. A sustainable option would be the use of a ceramic separator, which not only has proven to be suitable as electrodes separator in microbial fuel cells (MFCs) and is compatible with long-term operations, but it would also provide structural support to the system [19, 20].

Several parameters in the soil, such as porosity, water content, amount of organic matter and composition, and in the presence of contaminants, their type and concentration, can have a marked effect on the electrochemical performance of a SMFC [21]. In particular, water content in soil is a key factor; microorganisms require specific conditions of moisture

to be alive and able to degrade organic substrates [22]. Water is also involved in the transport of ions through the soil, with vanishing ion diffusion rates under low content of water [23]. An in-depth investigation on the movement of water in the soil surrounding a SMFCs is therefore very important. When the soil pores are filled with water, a single-phase gravity driven flow prevails, while other phenomena may occur in unsaturated systems, such as osmosis and capillarity [24].

In this study, a novel and low-cost tubular SMFC for soil bioremediation is proposed. A terracotta tube is used to separate the anode from the cathode. To reach increasing soil depths and easily scale-up the system for in field applications, a modular design is developed by piling together several tubular SMFCs. To assess the impact of operational conditions, such as soil type and temperature, on the performance of the piled SMFCs, and to guide on practical implementations, a mathematical model is proposed. The model, calibrated by experimental data, predicts the performance of the SMFCs pile by combining transport phenomena in the solid, liquid and gas phase with (bio)electrochemical reactions, charge balance, evaporation and transport of water and its effect on transport of solutes. The model is also used to predict the efficacy of the piled SMFCs to biodegrade an exemplary persistent organic pesticide, such as hexachlorobenzene, was also modelled. While modelling has been already applied to predict the performance of electroactive biofilm in MFCs [25, 26], and of MFCs under either batch [27] or flow conditions [28, 29], and in stacks [30], to the best of the authors' knowledge, this is the first model reported for a SMFC. For the first time, (bio)electrochemical processes are combined with the effect of water content on transport of solutes in soils and porous matrix, to provide a useful guide on operational conditions and scale-up strategies of SMFCs in bioremediation.

2. Materials and Methods

2.1 Materials

All chemicals, purchased from Alfa Aesar and Sigma-Aldrich, were of analytical grade and used without further modification unless otherwise specified. All aqueous solutions were prepared with ultrapure water (18.2 MΩ cm^{-1}) from a Milli-Q system (Millipore, UK). The soil was collected from the University of Bath campus (51°22'34.9"N, 2°19'31.2"W), and cleared from any stone, twig, and root. The moisture content of the soil was assessed by calculating the difference in weight of a sample before, W_1 (g), and after, W_2 (g), incubation at 105 °C for 24 h according to [31]:

$$\text{Moisture content } (\%) = \left(\frac{W1-W2}{W2}\right) \times 100 \qquad \textit{(Eq.1)}$$

The percentage of organic matter in the soil was determined by the loss of weight on ignition method [31]:

$$\text{Percentage organic matter } (\%) = \left(\frac{W2-W3}{W2}\right) \times 100 \qquad \textit{(Eq.2)}$$

where W_3 (g) is the weight of dry soil sample after incubation at 400 °C for 4 h.

The conductivity and pH of the soil were measured with direct measurement meter (Thermo Scientific Orion Star A325 probe). Table 1 summarises the physicochemical properties of the soil used in the experiments.

2.2 Tubular SMFCs design and construction of system

The SMFCs consisted of a terracotta hollow tube (inner diameter: 33 mm; thickness: 3 mm; 100 mm long), provided by Weston Mill Pottery Ltd, United Kingdom. The tube has the function to provide structural support to the SMFC while separating the anode from the cathode (Figure 1A). Both electrodes consisted of graphite felt (GF, 7 mm thickness, Online Furnace Services Ltd, United Kingdom). The anode (15 width × 8 height cm^2), pre-treated as previously reported [32], was wrapped around the outer part of the tube. A plastic mesh (Stallion-801-Gutter-G-Mesh-Pk3) was used to secure the anode to the terracotta tube. The

cathode (9 width × 8 height cm^2) was wrapped around the inner part of the terracotta tube, at the same height of the anode, and secured with the plastic mesh (N2530, Industrial Netting, MN, USA). Titanium wire (0.25 mm diameter, Alfa Aesar, United Kingdom), used as the current collector, was threaded into electrode, and coated with plastic tube for insulation.

Three tubular SMFCs, named as $SMFC_T$, $SMFC_M$ and $SMFC_B$, were piled together, with a gap between each other of 2 cm, obtained with the use of a rubber (Nitrile Rubber Seal, RS Components Ltd, United Kingdom), so that $SMFC_T$ would be at the top of the pile, $SMFC_M$ in the middle and $SMFC_B$ at the bottom. Three resulting piles were placed into a plastic bucket (height: 45 cm; base diameter: 27 cm) filled with soil, so that the anodes would face the soil and the cathodes would be exposed to air, as shown in Fig 1C. As shown, the anode of $SMFC_T$ was at a depth of 6 cm to 14 cm from the soil surface, $SMFC_M$ was at a depth of 16 to 24 cm from the soil surface, and $SMFC_B$ at a depth of 26 to 34 cm from the soil surface.

2.3. Experimental set-up and operation

To allow acclimation and enrichment of electroactive microorganisms onto the anode surface, the SMFCs were operated in close circuit mode under an external resistance of 500 Ω for three weeks. During this time, the cell voltage was monitored with a data acquisition system (DAQ6510/7700, Keithley Instrument Inc., USA) at a frequency of 1 min. After three weeks, polarization tests were performed to assess the electrochemical performance of the fuel cells. For these tests, the SMFCs were operated in open circuit voltage (OCV) mode until a stable voltage was generated (approximately after 1 hour), and then connected to a resistor box (Cropico RM6 Decade) to step-decrease the applied external load from 100,000 Ω to 10 Ω. To monitor the anode potential, an Ag/AgCl reference electrode (BASi MF-2052, Bioanalytical Systems Inc., USA) was positioned in the soil, in proximity to the anodes, while the cathode potential was derived from the cell potential and the anode potential. The current (I) was calculated using the Ohm's law (V=I R), where R is the applied external resistance.

The power (P) was calculated based on Joule's first law. The internal resistance was calculated according to the electrode potential slope method [33]. To calculate the ohmic resistance, the slope was calculated within the range 1,000 - 10 Ω to ensure significant R^2 value (> 0.99). During operation, the soil was watered with approximately 250 ml of tap water every 24 hrs.

2.4 Model description

The mathematical model was implemented and solved with the COMSOL Multiphysics© software. Both experimental data and data from the literature (summarised in Table 2) were used to calibrate the model. Charge balances and mass balances of water and chemical species involved in the process, along with the relevant equations for electrochemical and bioelectrochemical reactions were used for the model. The system (soil and piled SMFCs) was modelled with solid and gas phase integration domains. Exploiting the axial symmetry of the system, six rectangular domains were used, as shown in Figure 1B:

- Domain 1: soil, where transport of water and chemical species through a porous matrix occurs.
- Domain 2: porous anode, where biofilm grows and bioelectrochemical processes generate electricity.
- Domain 3: separator, a porous matrix where water and chemical species move throughout.
- Domain 4: porous cathode, with consumption of protons by oxygen reduction reactions and water evaporation.
- Domains 5 and 6 represent the inner part of the tube and the layer of air over the soil surface.

The model was developed with the following assumptions:

- The organic matter of the soil was modelled considering with two key components: 1) the natural organic matter of the soil at high concentration, representing the main substrate for the growth of the anodic biofilm; 2) a recalcitrant organic pollutant, such as hexachlorobenzene.
- Microorganisms are modelled with the lumped variables M_S (suspended) and M_A (adhered).
- The content of natural organic matter and free bacteria in the soil is constant with time, only the pollutant concentration changes as a result from transport to/degradation at the anode
- Biofilm formation starts from nucleation of suspended microorganisms onto the surface of the anode, where growth occurs. A conduction-based approach was used to describe the mechanism of electron transfer in the biofilm. This approach has been previously proposed to describe the kinetics of bioelectrochemical reactions in microbial fuel cells [34]. Cells nucleation and growth are described using a Nernst-Monod kinetics, which relates the rate of electron donor (i.e. organic matter) utilization with the electron donor concentration and electrical potential in biofilms, as previously suggested [35]
- Water flow in soil was described by the Richards' equation, which combines the Darcy–Buckingham's equation for the flux with mass conservation [36]. The Richards' equation allows the characterisation of the water flow in soil through a diffusion-like equation (Equation 4) with water diffusivity that depends on soil properties [37].
- Water moves by capillary flow throughout the anode, the porous ceramic separator and the cathode. Though the separator, water flow in both liquid or vapour phase depends on diffusion rates of vapour and liquid water and on porosity [38]. In materials with high and uncontrolled porosity, such as terracotta, diffusion of water in liquid phase can be assumed as the dominant mechanism [39]. In such materials as

carbon felt or clothes, when exposed to air diffusion of water mainly occurs by capillary flow of liquid water driven by evaporation [40]. In particular, at the surface of the cathode, equilibrium conditions are established between water in the liquid and vapour phase, with partial pressure of water in air equal to the vapour pressure. The evaporation rate E_R (mol m^{-3} s^{-1}) can be written as a function of partial pressures at the interface carbon fibre/air $P_{W_{sat}}$ and in the bulk air P_W:

$$E_R = h_W a_{Cat}(P_{W_{sat}} - P_W) \qquad \textit{(Eq. 3)}$$

where h_W (mol m^{-2} s^{-1} Pa^{-1}) is the coefficient of water evaporation and a_{Cat} (m^{-1}) is the cathode specific surface.

Mass balances were written in the relevant domains for water and all the involved species.

In the soil, transport of water and chemicals can be described as follows:

$$\varepsilon_{Soil}\frac{\partial C_i}{\partial t} + \nabla \cdot \left(-\mathcal{D}_{i,Soil}\nabla C_i\right) = 0 \qquad \textit{(Eq. 4)}$$

Where: C_i (mol m^{-3}) is the concentration of the ith species in pores; ε_{Soil} is the soil porosity; $\mathcal{D}_{i,Soil}$ (m^2 s^{-1}) is the diffusivity of the ith species in soil. Water diffusivity depends on the water content and soil properties [24]. The fluid diffusivities have been determined by considering the percolation theory [41].

At the anode, species of interest are the organic substrates, M_s, M_a, water W and H^+. Their initial concentration is nil. The transport across the anode depends on diffusivity and reactions as follow:

$$\varepsilon_{An}\frac{\partial C_i}{\partial t} + \nabla \cdot \left(-\mathcal{D}_{i,An}\nabla C_i\right) = R_{i,An} \qquad \textit{(Eq. 5)}$$

Where ε_{An} (-) is the anode porosity and $\mathcal{D}_{i,An}$ (m^2 s^{-1}) is the diffusivity of the ith species in the porous anode. Constant value of porosity was assumed. This is indeed a common

assumption in microbial fuel cell modelling, used recently for a brush [42] and for a carbon felt [43] electrode, with uniform distribution of microbial populations in the anodic compartment. Constant values are used to avoid increase in complexity of the model without adding significant improvement in results accuracy [44-46]. The reaction terms $R_{i,An}$ (mol m^{-3} s^{-1}) can be defined as:

$$R_{OM,An} = -(r_1 + r_2) \quad \textit{(Eq. 6)}$$

$$R_{M_S,An} = -\upsilon_{OM}\, r_1 \quad \textit{(Eq. 7)}$$

$$R_{M_A,An} = r_1 + r_2 - r_3 \quad \textit{(Eq. 8)}$$

$$R_{H^+,An} = \upsilon_{H^+}(r_1 + r_2) \quad \textit{(Eq. 9)}$$

$$R_{W,An} = 0 \quad \textit{(Eq. 10)}$$

Where: r_1 (mol m^{-3} s^{-1}) is the rate of biofilm nucleation; r_2 (mol m^{-3} s^{-1}) is the growth rate; r_3 (mol m^{-3} s^{-1}) is the rate of inactivation. r_1, r_2 and the reaction term related to the organic pollutant, R_{OP}, were described with the Nernst-Monod kinetics [27, 47, 48]:

$$r_1 = k_1 \frac{C_{OM}}{C_{OM} + K_{s,s}} \frac{C_{Ms}}{C_{Ms} + K_{s,Ms}} \left[1 + exp\left(-\frac{F}{RT}\eta_{An}\right)\right]^{-1} \quad \textit{(Eq. 11)}$$

$$r_2 = k_2 \frac{C_{OM}}{C_{OM} + K_{s,A}} \frac{C_{M_A}}{C_{M_A} + K_{s,M_A}} \left[1 + exp\left(-\frac{F}{RT}\eta_{An}\right)\right]^{-1} \quad \textit{(Eq. 12)}$$

$$R_{OP} = k_3 C_{OP} \frac{C_{M_A}}{C_{M_A} + K_{s,M_A}} \left[1 + exp\left(-\frac{F}{RT}\eta_{An}\right)\right]^{-1} \quad \textit{(Eq. 13)}$$

Where: k_1, k_2 (mol m^{-3} s^{-1}) and k_3 (s^{-1}) are the specific reaction rates; $K_{s,s}$, $K_{s,A}$, $K_{s,Ms}$ and K_{s,M_A} (mol m^{-3}) are the half saturation constants; η_{An} (V) is the anodic overpotential.

The inactivation term r_3 follows a pseudo-first order law [29]:

$$r_3 = k_d C_{M_A} \qquad \textit{(Eq. 14)}$$

Where k_d (s^{-1}) is the inactivation rate constant for biofilm.

The diffusivity of solutes, $\mathcal{D}_{i,j}$, in porous media depends on the water content and it can be determined from the diffusivity of solute in water, $\mathcal{D}_i$, with the following equation [23]:

$$\mathcal{D}_{i,j} = 1.1\, \mathcal{D}_i C_W (C_W - C_{W_c}) \qquad \textit{(Eq. 15)}$$

Where C_{W_c} (mol m^{-3}) is the threshold water content for vanishing of solute diffusivity and 1.1 is a factor describing the meandering of the diffusive pathway [49].

Through the **ceramic separator**, species diffuse according to:

$$\varepsilon_{sep} \frac{\partial C_i}{\partial t} + \nabla \cdot \left(-\mathcal{D}_{i,sep} \nabla C_i\right) = 0 \qquad \textit{(Eq. 16)}$$

Where ε_{Sep} (-) is the separator porosity and $\mathcal{D}_{i,Sep}$ ($m^2\ s^{-1}$) is the diffusivity of the i^{th} species through the separator.

At the cathode, the transport reaction equation is:

$$\varepsilon_{Cat} \frac{\partial C_i}{\partial t} + \nabla \cdot \left(-\mathcal{D}_{i,Cat} \nabla C_i\right) = R_{i,Cat} \qquad \textit{(Eq. 17)}$$

Where ε_{Cat} (-) is the cathode porosity and $\mathcal{D}_{i,Cat}$ ($m^2\ s^{-1}$) is the diffusivity of the i^{th} species through the cathode. The reaction terms $R_{i,Cat}$ (mol $m^{-3}\ s^{-1}$) are defined as:

$$R_{W,Cat} = -E_R \qquad \textit{(Eq. 18)}$$

$$R_{H^+,Cat} = -\frac{I_{Cat}}{F} \qquad \textit{(Eq. 19)}$$

The consumption of protons $R_{H^+,Cat}$ depends on the cathodic current I_{Cat} (A m^{-3}), defined with a Butler-Volmer equation [25]:

$$I_{Cat} = I_{Cat}^{0}\, exp\left(-0.5\frac{F}{RT}\eta_{Cat}\right) \qquad \textit{(Eq. 20)}$$

Where η_{Cat} (V) is the cathodic overpotential. The exchange current I_{Cat}^{0} (A m^{-3}) depends on the flux of ions throughout the separator and on the catalytic properties of the material, according to:

$$I_{Cat}^{0} = -k_{H_2}\, D_{H^+,Sep} \nabla C_{H^+} \qquad \textit{(Eq. 21)}$$

In the **gas phase domains** water evaporating from cathode and soil diffuses according to:

$$\frac{\partial \mathrm{C_{W_{vap}}}}{\partial \mathrm{t}} + \nabla \cdot \left(-\mathcal{D}_{\mathrm{Vap}} \nabla \mathrm{C_{W_{vap}}}\right) + E_R = 0 \qquad \textit{(Eq. 22)}$$

Where $\mathcal{D}_{\mathrm{Vap}}$ (m^2 s^{-1}) is the water vapour diffusivity.

Charge conservation in the SMFC is described using a Poisson's Law [28]:

$$\nabla \cdot \left(-\sigma_{\mathrm{j}} \nabla \mathrm{V_j}\right) = \mathrm{f_j} \qquad \textit{(Eq. 23)}$$

Where σ_{j} (S m^{-1}) is the electric conductivity and $\mathrm{f_j}$ (A m^{-3}) is the current source. j refers to either anode (An), separator (Sep) or cathode (Cat). Equation 23 has been applied separately to domains 2-4. In the anodic region, the term $\mathrm{f_j}$ correspond to a current source I_{An} (A m^{-3}) defined as [28]:

$$\mathrm{I_{AN}} = \mathrm{r_2\, z_{AN} F} \qquad \textit{(Eq. 24)}$$

Where $\mathrm{z_{AN}}$ is the number of the electrons involved in the degradation of organic matter.

The model equations were numerically solved with the following boundary conditions:

- Soil-anode boundary: continuity of concentration of chemical species, water and microorganisms in Equations 4 and 5 ($\mathrm{C_{i,AN}} = \mathrm{C_{i,Soil}}$); electric ground ($\mathrm{V} = 0$).
- Anode-separator boundary: continuity of concentration of chemical species and water, no flux of microorganisms in Equations 5 and 16 ($\nabla \mathrm{C}_i = 0$); continuity of electric field in Equation 23.
- Separator-cathode boundary: continuity of concentration of chemical species and water (Equations 16 and 17); continuity of electric field (Equation 23).
- External boundaries: no flux of species ($\nabla \mathrm{C}_i = 0$) and charge ($\nabla V = 0$).

3. Results and Discussion

The model was calibrated by using experimental data generated from the enrichment of the anodic biofilm of the tubular SMFCs. The three SMFCs piled together as shown in Figure 1C, were immerged in the soil and the cell voltage was monitored with the time. Figure 2A compares the experimental data obtained with the data predicted by the model.

As shown, the performance of the SMFCs varies with the soil depth. While the lag phase is the same for all the SMFCs, the exponential phase is characterised by a different slope for each of them (4.56 mV d^{-1}, R^2=0.99 for $SMFC_T$, 6.8 mV d^{-1}, R^2=0.95 for $SMFC_M$, 7.6 mV d^{-1}, R^2=0.98 for $SMFC_B$). The value of the steady-state output voltage is also different. $SMFC_B$, which is placed in the deepest part of the soil, generates the highest cell voltage, which is about twice higher than the voltage generated by $SMFC_T$, placed in the shallowest part of the soil. Polarisation tests performed on the SMFCs after the enrichment, and the derived power curves confirm this result; the peak power generated by $SMFC_B$ is approximately twice higher than the peak power generated by $SMFC_B$ (Figure 2B). An investigation on the electrode potentials, suggests that this difference may be caused by the cathode. As shown in Figure 2C, while the electrode potential of the anodes is unchanged in the three SMFCs, the cathodic potential varies. In particular, the region showing difference with the soil depth

is the one affected by the internal resistance. The values of the internal resistance calculated for each SMFCs based on the electrode potential monitoring during the polarization test were of 1,044 Ω for $SMFC_T$, 948 Ω for $SMFC_M$, and 698 Ω for $SMFC_B$. The internal resistance of an MFC is the result of the nature of electrode, electrolyte and current collector. Since the materials used for the piled SMFCs are the same, the only factor that would vary among the three and affect the internal resistance is the electrolyte. The difference in the internal resistance may be the consequence of an uneven distribution of water in the soil and a consequent difference in the cathode wetness. This difference would result in a change on both electrode conductivity and junction resistance between cathode and ceramic separator, as previously suggested [15, 22].

The mathematical model developed was used to predict the effect of soil dewatering and consequent drying of the cathode on the performance of the three SMFCs in the pile, under two different temperatures, and with soils characterised by a different diffusivity of water. The parameters were set-up to represent soils with high content of sand similar to that used in the experiment (D_W = 6 cm^2 min^{-1}), and loam (D_W = 0.8 cm^2 min^{-1}) [24].

Another important factor is the evaporation rate, which is a function of temperature (Equation 3) and regulates the exchange of heat between soil surface and atmosphere. Values of soil temperatures may be considerably different with season and latitudes, and the model can be used to predict the effect of such changes in water content. In this work, simulations were done with evaporation rates corresponding to the temperature of 25°C and 40°C, with a background humidity of 10%. The ability of SMFC technology to remediate soils has been so far demonstrated only under a temperature range of 25-30°C [8]. Barbato et al [50] has previously investigated the performance of a single chamber MFC for wastewater treatment within a much wider range of 5 - 35°C, showing that at low temperatures the system required a longer start-up time, and reached a power output up to one fifth lower than the value

obtained at 35 °C. It has been shown that temperatures lower than 15°C severely limit biofilm growth on carbon-based anodes [50, 51], and generate unstable power outputs [52]. As such, the two temperatures considered in this study (25°C and 40°C) lie within the optimal operating temperature range for MFCs, associated with stable performance [50, 52, 53].

Figure 3 shows the effect that both the evaporation rate and the diffusion coefficient of water have on the content of water in the soil and, consequently on the performance of the three SMFCs in the pile. The numerical solution starts from saturation values at time zero, with water homogeneously distributed in the soil pores, up to simulate 20 days of treatment.

The model predicts an initial transient behaviour. After approximately 40 h of operation, no significant variations with time in the water profile are observed. The parameters used to obtain the data in Figure 3A refer to the same conditions of the lab experiments. As shown, the cathode of $SMFC_T$ is dryer than the other two, in line with the hypothesis that the moisture content is the factor affecting this SMFC. On the other hand, the effect of a higher temperature (40 °C) is more marked for the case of a soil with low diffusivity of water, ultimately leading to full drying of the cathode in the three SMFCs (Figure 3B).

The corresponding predictions of the output voltage generated by the three SMFCs are reported in Figure 4. As shown, under high evaporation rate conditions, the drying of cathodes and separators strongly affects the generation of electricity. This effect is reduced when the soil is characterised by a high diffusivity of water, which would guarantee homogeneous performances at the different soil depths. Figure 4 (bottom) also shows the output voltage generated by the three SMFCs in the pile over time for the two types of soil and at the two temperatures considered. The dryer is the cathode, at low water diffusivity and high temperature, the poorer the performance of the SMFC. As already observed, at low water diffusivity (Figure 4C) the voltage generated by the three SMFCs is very poor also at moderate evaporation rates. On the other hand, for larger water diffusivity, a marked

difference in the output voltage between $SMFC_B$ and $SMFC_T$ is observed at high evaporation rates.

Once calibrated with the experimental data and used to justify the difference in performance along the soil depth, the model was subsequently used to predict the performance of the SMFCs for the bioremediation of a recalcitrant pollutant. Hexachlorobenzene was used as the model pollutant, since it is one of the most studied environmental pollutant worldwide. Classified as carcinogenic and a persistent organic pollutant, because of its very slow degradation rate, its use as pesticide has been banned in 1995 [2]. Nonetheless, hexachlorobenzene can still be abundantly present in soil and sediments, since it can be produced as a by-product in the manufacture of organic chemicals and in the burning of municipal waste [54]. The use of MFC technology to degrade hexachlorobenzene in soil has been recently reported. The authors observed a degradation rate over 6 times faster with the MFC, thanks to the action of the electrons generated by the electrogenic bacteria [13]. For the simulation, kinetic parameters were taken from this study [13], and accordingly the process of pollutant degradation was modelled as simultaneous to generation of electricity by the SMFCs, under an initial concentration of 35 mg kg^{-1} of the pollutant was considered. Literature values of C_{W_c} in Equation 15 were used, which are typical of sandy ($C_{W_c} = 0$) and loam ($C_{W_c} = 0.15$) soils [55]. Figures 5 reports the model predictions in terms of pollutant concentration with time. As shown, the rapid drop in the pollutant concentration in soil observed during the initial treatment period was followed by a slower decay. This behaviour is in line with what previously experimentally observed [13].

The efficacy of pollutant removal varies along the SMFCs pile, as it can be observed in Figures 6 and 7. The areas corresponding to low moisture content, as per Figure 3, are associated with no pollutant removal, due to the consequent poor mobility of chemical species [55]. Moreover, as expected, a high pollutant removal occurs in the soil adjacent to

the anode, where the electroactive bacteria act, with a low to null removal in the bulk of the soil. The 1D profiles of hexachlorobenzene removal as a function of the distance from the anode generated by the model, shown in Figure 7, allow the prediction of an effective distance of pollutant removal from the anode or distance of influence. Mobility and bioavailability of pollutants are limited by the soil characteristics and depending on the nature of the target pollutant, the effective distance may be limited to only few centimetres from the electrode surface [56]. An effective distance less than 1 cm was observed for petroleum hydrocarbons removal in saline soils [22]. Under the conditions simulated by our model, the effective distance for the SMFCs pile was estimated to be of 2.5 cm for the case of a soil with a good water diffusivity (A and B scenarios), and less than 2 cm for a soil with poor water diffusivity (C scenario) and for $SMFC_T$ under high evaporation rates (B scenario). Based on these results, an effective way to treat homogeneously a polluted soil, under the conditions considered for the model, would be to generate an array of SMFCs piles placed at a distance of 4 (C scenario) or 5 cm (A and B scenarios), depending on the soil considered. Consequently, this model can vehicle the designs of strategic arrays of SMFCs piles for the effective bioremediation of a target contaminated land. The versatile nature of the model allows the easy adaptation to different types of soils and pollutants.

4. Conclusions

SMFCs have great potential for the bioremediation of recalcitrant pollutants in soil. In this study, an innovative SMFC design is provided that can be easily scaled-up in field applications, because of both its simplicity and the possibility to customise the depth of action by piling up several SMFC units together. The versatile mathematical model developed in this study can help predict the performance of the SMFCs pile according to soil properties and allows the development of strategic design of arrays of SMFCs piles for effective bioremediation of contaminated soils. The numerical solutions generated by the

model provide a prediction on space and time concentration profiles of the organic compounds in soil to be treated and can therefore assist on effective implementations of the SMFCs pile. Our model can consequently become a fundamental guide for scale-up bioremediation strategies by SMFCs.

Acknowledgements

This work is part of the project GREENER that has received funding from the European Union's Horizon 2020 research and innovation programme under the grant agreement No 826312

References

[1] C. Carlon, L. Pizzol, A. Critto, A. Marcomini, A spatial risk assessment methodology to support the remediation of contaminated land, Environment International 34(3) (2008) 397-411.
[2] E. Morillo, J. Villaverde, Advanced technologies for the remediation of pesticide-contaminated soils, Science of the Total Environment 586 (2017) 576-597.
[3] U. Ali, J.H. Syed, R.N. Malik, A. Katsoyiannis, J. Li, G. Zhang, K.C. Jones, Organochlorine pesticides (OCPs) in South Asian region: a review, Science of the Total Environment 476 (2014) 705-717.
[4] R.G. Lacalle, J.D. Aparicio, U. Artetxe, E. Urionabarrenetxea, M.A. Polti, M. Soto, C. Garbisu, J.M. Becerril, Gentle remediation options for soil with mixed chromium (VI) and lindane pollution: biostimulation, bioaugmentation, phytoremediation and vermiremediation, Heliyon 6(8) (2020) e04550.
[5] A. Cundy, R. Bardos, A. Church, M. Puschenreiter, W. Friesl-Hanl, I. Müller, S. Neu, M. Mench, N. Witters, J. Vangronsveld, Developing principles of sustainability and stakeholder engagement for “gentle” remediation approaches: The European context, Journal of environmental management 129 (2013) 283-291.
[6] Y. Wu, X. Jing, C. Gao, Q. Huang, P. Cai, Recent advances in microbial electrochemical system for soil bioremediation, Chemosphere 211 (2018) 156-163.
[7] D. Borello, G. Gagliardi, G. Aimola, V. Ancona, P. Grenni, G. Bagnuolo, G.L. Garbini, L. Rolando, A.B. Caracciolo, Use of microbial fuel cells for soil remediation: A preliminary study on DDE, International Journal of Hydrogen Energy (2020).
[8] X. Li, X. Wang, L. Weng, Q. Zhou, Y. Li, Microbial fuel cells for organic-contaminated soil remedial applications: A review, Energy Technology 5(8) (2017) 1156-1164.
[9] P.A. Castresana, S.M. Martinez, E. Freeman, S. Eslava, M. Di Lorenzo, Electricity generation from moss with light-driven microbial fuel cells, Electrochimica Acta 298 (2019) 934-942.
[10] L. Lu, T. Huggins, S. Jin, Y. Zuo, Z.J. Ren, Microbial metabolism and community structure in response to bioelectrochemically enhanced remediation of petroleum hydrocarbon-contaminated soil, Environmental science & technology 48(7) (2014) 4021-4029.

[11] D. Mao, L. Lu, A. Revil, Y. Zuo, J. Hinton, Z.J. Ren, Geophysical monitoring of hydrocarbon-contaminated soils remediated with a bioelectrochemical system, Environmental Science & Technology 50(15) (2016) 8205-8213.
[12] D.-Y. Huang, S.-G. Zhou, Q. Chen, B. Zhao, Y. Yuan, L. Zhuang, Enhanced anaerobic degradation of organic pollutants in a soil microbial fuel cell, Chemical engineering journal 172(2-3) (2011) 647-653.
[13] X. Cao, H.-l. Song, C.-y. Yu, X.-n. Li, Simultaneous degradation of toxic refractory organic pesticide and bioelectricity generation using a soil microbial fuel cell, Bioresource Technology 189 (2015) 87-93.
[14] X. Cao, C. Yu, H. Wang, F. Zhou, X. Li, Simultaneous degradation of refractory organic pesticide and bioelectricity generation in a soil microbial fuel cell with different conditions, Environmental technology 38(8) (2017) 1043-1050.
[15] Y. Li, X. Li, Y. Sun, X. Zhao, Y. Li, Cathodic microbial community adaptation to the removal of chlorinated herbicide in soil microbial fuel cells, Environmental Science and Pollution Research 25(17) (2018) 16900-16912.
[16] J. Dziegielowski, B. Metcalfe, P. Villegas-Guzmán, C. Martínez-Huitle, A. Gorayeb, J. Wenk, M. Di Lorenzo, Development of a functional stack of soil microbial fuel cells to power a water treatment reactor: from the lab to field trials in North East Brazil. Journal of Applied Energy, Journal of Applied Energy (2020).
[17] L. Lu, H. Yazdi, S. Jin, Y. Zuo, P.H. Fallgren, Z.J. Ren, Enhanced bioremediation of hydrocarbon-contaminated soil using pilot-scale bioelectrochemical systems, Journal of hazardous materials 274 (2014) 8-15.
[18] K. Wetser, K. Dieleman, C. Buisman, D. Strik, Electricity from wetlands: Tubular plant microbial fuels with silicone gas-diffusion biocathodes, Applied energy 185 (2017) 642-649.
[19] M. Behera, P.S. Jana, M. Ghangrekar, Performance evaluation of low cost microbial fuel cell fabricated using earthen pot with biotic and abiotic cathode, Bioresource technology 101(4) (2010) 1183-1189.
[20] I. Gajda, O. Obata, M.J. Salar-Garcia, J. Greenman, I.A. Ieropoulos, Long-term bio-power of ceramic Microbial Fuel Cells in individual and stacked configurations, Bioelectrochemistry 133 (2020) 107459.
[21] X. Zhang, X. Li, X. Zhao, Y. Li, Factors affecting the efficiency of a bioelectrochemical system: a review, RSC Advances 9(34) (2019) 19748-19761.
[22] X. Wang, Z. Cai, Q. Zhou, Z. Zhang, C. Chen, Bioelectrochemical stimulation of petroleum hydrocarbon degradation in saline soil using U-tube microbial fuel cells, Biotechnology and Bioengineering 109(2) (2012) 426-433.
[23] A. Hunt, R. Ewing, On the vanishing of solute diffusion in porous media at a threshold moisture content, Soil Science Society of America Journal 67(6) (2003) 1701-1702.
[24] W. Gardner, Mathematics of isothermal water conduction in unsaturated soils, Highway research board special report 40 (1956) 78-87.
[25] C. Picioreanu, I.M. Head, K.P. Katuri, M.C. van Loosdrecht, K. Scott, A computational model for biofilm-based microbial fuel cells, Water research 41(13) (2007) 2921-2940.
[26] B. Korth, L.F. Rosa, F. Harnisch, C. Picioreanu, A framework for modeling electroactive microbial biofilms performing direct electron transfer, Bioelectrochemistry 106 (2015) 194-206.
[27] M.M. Mardanpour, S. Yaghmaei, M. Kalantar, Modeling of microfluidic microbial fuel cells using quantitative bacterial transport parameters, Journal of Power Sources 342 (2017) 1017-1031.
[28] F. Hashemi, S. Rowshanzamir, M. Rezakazemi, CFD simulation of PEM fuel cell performance: Effect of straight and serpentine flow fields, Mathematical and Computer Modelling 55(3) (2012) 1540-1557.

[29] Y. Zeng, Y.F. Choo, B.-H. Kim, P. Wu, Modelling and simulation of two-chamber microbial fuel cell, Journal of Power Sources 195(1) (2010) 79-89.
[30] S. Mateo, M. Mascia, F.J. Fernandez-Morales, M.A. Rodrigo, M. Di Lorenzo, Assessing the impact of design factors on the performance of two miniature microbial fuel cells, Electrochimica Acta 297 (2019) 297-306.
[31] M. Motsara, R.N. Roy, Guide to laboratory establishment for plant nutrient analysis, Food and Agriculture Organization of the United Nations Rome2008.
[32] S.M. Martinez, M. Di Lorenzo, Electricity generation from untreated fresh digestate with a cost-effective array of floating microbial fuel cells, Chemical Engineering Science 198 (2019) 108-116.
[33] R. Rossi, B.P. Cario, C. Santoro, W. Yang, P.E. Saikaly, B.E. Logan, Evaluation of electrode and solution area-based resistances enables quantitative comparisons of factors impacting microbial fuel cell performance, Environmental science & technology 53(7) (2019) 3977-3986.
[34] C. Xia, D. Zhang, W. Pedrycz, Y. Zhu, Y. Guo, Models for Microbial Fuel Cells: A critical review, Journal of Power Sources 373 (2018) 119-131.
[35] A. Kato Marcus, C.I. Torres, B.E. Rittmann, Conduction-based modeling of the biofilm anode of a microbial fuel cell, Biotechnology and Bioengineering 98(6) (2007) 1171-1182.
[36] L.A. Richards, Capillary conduction of liquids through porous mediums, Physics 1(5) (1931) 318-333.
[37] G.J. Huffman, D.T. Bolvin, E.J. Nelkin, D.B. Wolff, R.F. Adler, G. Gu, Y. Hong, K.P. Bowman, E.F. Stocker, The TRMM multisatellite precipitation analysis (TMPA): Quasi-global, multiyear, combined-sensor precipitation estimates at fine scales, Journal of hydrometeorology 8(1) (2007) 38-55.
[38] I. Gómez, J.M. Sala, J.A. Millán, Characterization of Moisture Transport Properties for Lightened Clay Brick — Comparison Between Two Manufacturers, Journal of Building Physics 31(2) (2007) 179-194.
[39] S. Kam, L. Zerbo, J. Bathiebo, J. Soro, S. Naba, U. Wenmenga, K. Traoré, M. Gomina, P. Blanchart, Permeability to water of sintered clay ceramics, Applied Clay Science 46(4) (2009) 351-357.
[40] K.T. Cho, M.M. Mench, Coupled effects of flow field geometry and diffusion media material structure on evaporative water removal from polymer electrolyte fuel cells, International Journal of Hydrogen Energy 35(22) (2010) 12329-12340.
[41] A.G. Hunt, M. Sahimi, Flow, transport, and reaction in porous media: Percolation scaling, critical-path analysis, and effective medium approximation, Reviews of Geophysics 55(4) (2017) 993-1078.
[42] S. Gadkari, S. Gu, J. Sadhukhan, Two-dimensional mathematical model of an air-cathode microbial fuel cell with graphite fiber brush anode, Journal of Power Sources 441 (2019) 227145.
[43] R.P. Pinto, B. Srinivasan, M.F. Manuel, B. Tartakovsky, A two-population bio-electrochemical model of a microbial fuel cell, Bioresource Technology 101(14) (2010) 5256-5265.
[44] V.B. Oliveira, M. Simões, L.F. Melo, A.M.F.R. Pinto, A 1D mathematical model for a microbial fuel cell, Energy 61 (2013) 463-471.
[45] M. Quaglio, G. Massaglia, N. Vasile, V. Margaria, A. Chiodoni, G.P. Salvador, S.L. Marasso, M. Cocuzza, G. Saracco, F.C. Pirri, A fluid dynamics perspective on material selection in microbial fuel cell-based biosensors, International Journal of Hydrogen Energy 44(9) (2019) 4533-4542.
[46] K.M. Hernández-García, B. Cercado, F.A. Rodríguez, F.F. Rivera, E.P. Rivero, Modeling 3D current and potential distribution in a microbial electrolysis cell with

augmented anode surface and non-ideal flow pattern, Biochemical Engineering Journal 162 (2020) 107714.
[47] A. Kato Marcus, C.I. Torres, B.E. Rittmann, Conduction-based modeling of the biofilm anode of a microbial fuel cell, Biotechnology and bioengineering 98(6) (2007) 1171-1182.
[48] C.I. Torres, A.K. Marcus, P. Parameswaran, B.E. Rittmann, Kinetic experiments for evaluating the Nernst− Monod model for anode-respiring bacteria (ARB) in a biofilm anode, Environmental science & technology 42(17) (2008) 6593-6597.
[49] P. Moldrup, T. Olesen, T. Komatsu, P. Schjønning, D. Rolston, Tortuosity, diffusivity, and permeability in the soil liquid and gaseous phases, Soil Science Society of America Journal 65(3) (2001) 613-623.
[50] R.A. Barbato, K.L. Foley, J.A. Toro-Zapata, R.M. Jones, C.M. Reynolds, The power of soil microbes: Sustained power production in terrestrial microbial fuel cells under various temperature regimes, Applied Soil Ecology 109 (2017) 14-22.
[51] Y. Zhang, J. Sun, Y. Hu, Z. Wang, S. Li, Effects of periodically alternating temperatures on performance of single-chamber microbial fuel cells, International Journal of Hydrogen Energy 39(15) (2014) 8048-8054.
[52] S. Cheng, D. Xing, B.E. Logan, Electricity generation of single-chamber microbial fuel cells at low temperatures, Biosens Bioelectron 26(5) (2011) 1913-7.
[53] L.H. Li, Y.M. Sun, Z.H. Yuan, X.Y. Kong, Y. Li, Effect of temperature change on power generation of microbial fuel cell, Environmental Technology 34(13-14) (2013) 1929-1934.
[54] E.M.U. Zamora, Hexachlorobenzene, in: P. Wexler (Ed.), Encyclopedia of Toxicology2014, pp. 869-871.
[55] T. Olesen, P. Moldrup, T. Yamaguchi, D. Rolston, Constant slope impedance factor model for predicting the solute diffusion coefficient in unsaturated soil, Soil Science 166(2) (2001) 89-96.
[56] X. Cai, Y. Yuan, L. Yu, B. Zhang, J. Li, T. Liu, Z. Yu, S. Zhou, Biochar enhances bioelectrochemical remediation of pentachlorophenol-contaminated soils via long-distance electron transfer, Journal of Hazardous Materials 391 (2020) 122213.
[57] B. Korth, L.F.M. Rosa, F. Harnisch, C. Picioreanu, A framework for modeling electroactive microbial biofilms performing direct electron transfer, Bioelectrochemistry 106 (2015) 194-206.
[58] Y.-C. Kim, Diffusivity of bacteria, Korean Journal of Chemical Engineering 13(3) (1996) 282-287.
[59] W.R.W. Gardner, MATHEMATICS OF ISOTHERMAL WATER CONDUCTION IN UNSATURATED SOIL, Highway Research Board Special Report (1958).
[60] E.L. Cussler, Diffusion: Mass Transfer in Fluid Systems, Cambridge University Press, New York, 1997.

Table 1. Physicochemical properties of the used soil

Parameter	
pH	6.66
Conductivity (*μ*s cm^{-1})	551.2
Moisture content (%)	63
Organic matter content (%)	22.43

Table 2. Model parameters

Symbol	Value	Unit	Ref.
$\mathcal{D}_{OM}$	$1 \cdot 10^{-9}$	$m^2\ s^{-1}$	[57]
$\mathcal{D}_{H^+}$	$9 \cdot 10^{-9}$	$m^2\ s^{-1}$	[57]
$\mathcal{D}_{H^+,m}$	$5.3 \cdot 10^{-9}$	$m^2\ s^{-1}$	[57]
$\mathcal{D}_{M_S}$	$3 \cdot 10^{-10}$	$m^2\ s^{-1}$	[58]
$\mathcal{D}_{W}$	$6.67 \cdot 10^{-6}$	$m^2\ s^{-1}$	[59]
$\mathcal{D}_{W_{Vap}}$	$3 \cdot 10^{-5}$	$m^2\ s^{-1}$	[60]
k_1	$1 \cdot 10^{-8}$	$mol\ m^{-3}\ s^{-1}$	This work
k_2	$5 \cdot 10^{-3}$	$mol\ m^{-3}\ s^{-1}$	This work
$k_{d,A}$	1	d^{-1}	This work
$K_{s,A}$	72	$mol_C\ m^{-3}$	This work
K_{s,M_A}	60	$mol_C m^{-3}$	This work
K_{s,M_S}	10	$mol_C m^{-3}$	This work
$K_{s,S}$	72	$mol_C m^{-3}$	This work

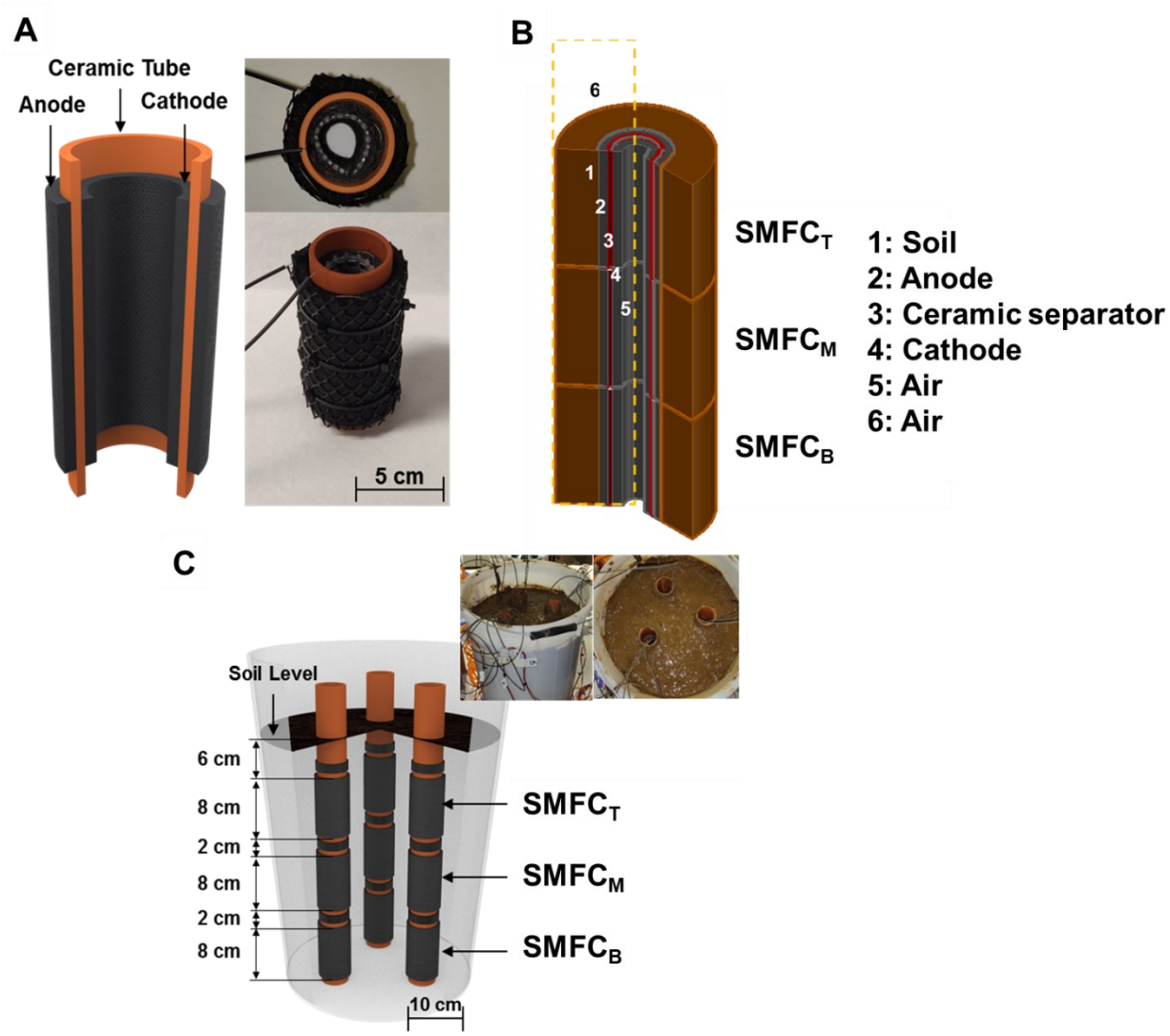

Figure 1. Tubular SMFC developed and arrangement in piles. A) SMFC design and actual photograph. B) Sketch of the simplified geometry used for modelling, with domains (1-6) of integration: 1: Soil; 2: Anode; 3: Ceramic separator; 4: Cathode; 5-6: Air. The dashed line refers to the contour of the surface plots in Figure 3, Figure 4, and Figure 6. C) Piles of three SMFCs and operational set-up.

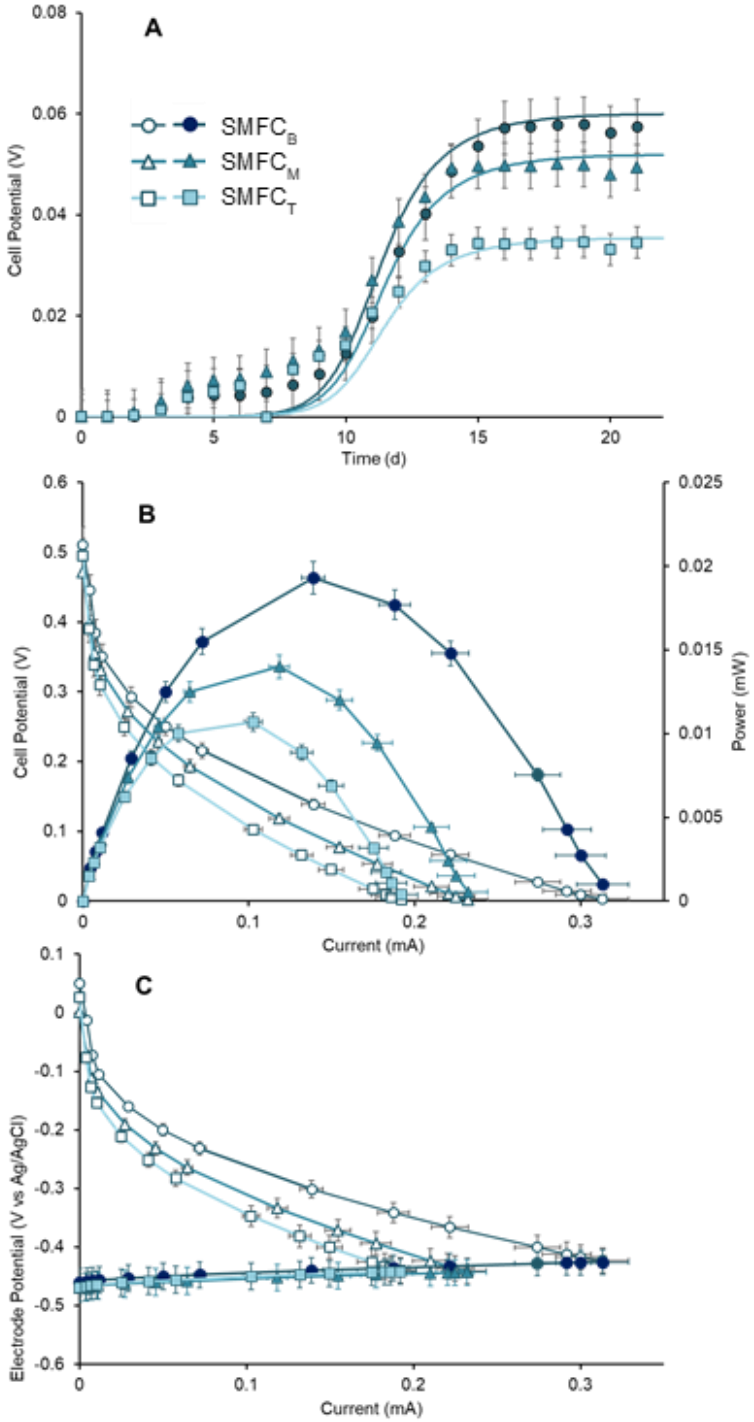

Figure 2. Enrichment curves and Polarisation tests on the piled SMFCs. A) Enrichment curves under an external resistance of 500 Ω. Comparison between experimental data (symbols) and data predicted by the model (lines) enrichment curves. B) Polarisation curve (empty symbols) and power curves (full symbols) for the piled SMFCs. C) Evolution with current of cathode (empty symbols) and anode potentials (full symbols) during the polarization test. Experimental data are the average of three replicates.

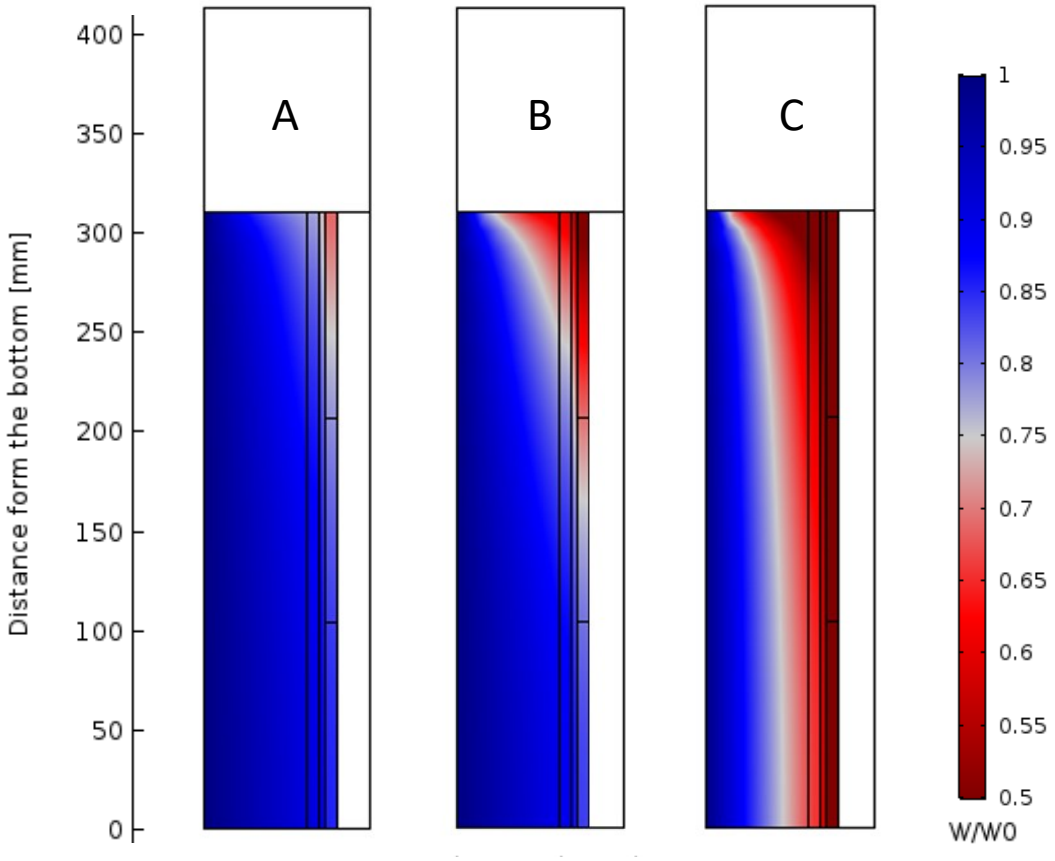

Figure 3. Space profiles of water content in the soil surrounding the SMFCs, (normalized by the initial content of water W_0), for different types of soil and at different temperatures as predicted by the model. A) D_W = 6 cm^2 min^{-1} and T = 25 °C. B) D_W = 6 cm^2 min^{-2} and T = 40 °C. C) D_W = 0.8 cm^2 min^{-2} and T = 25 °C.

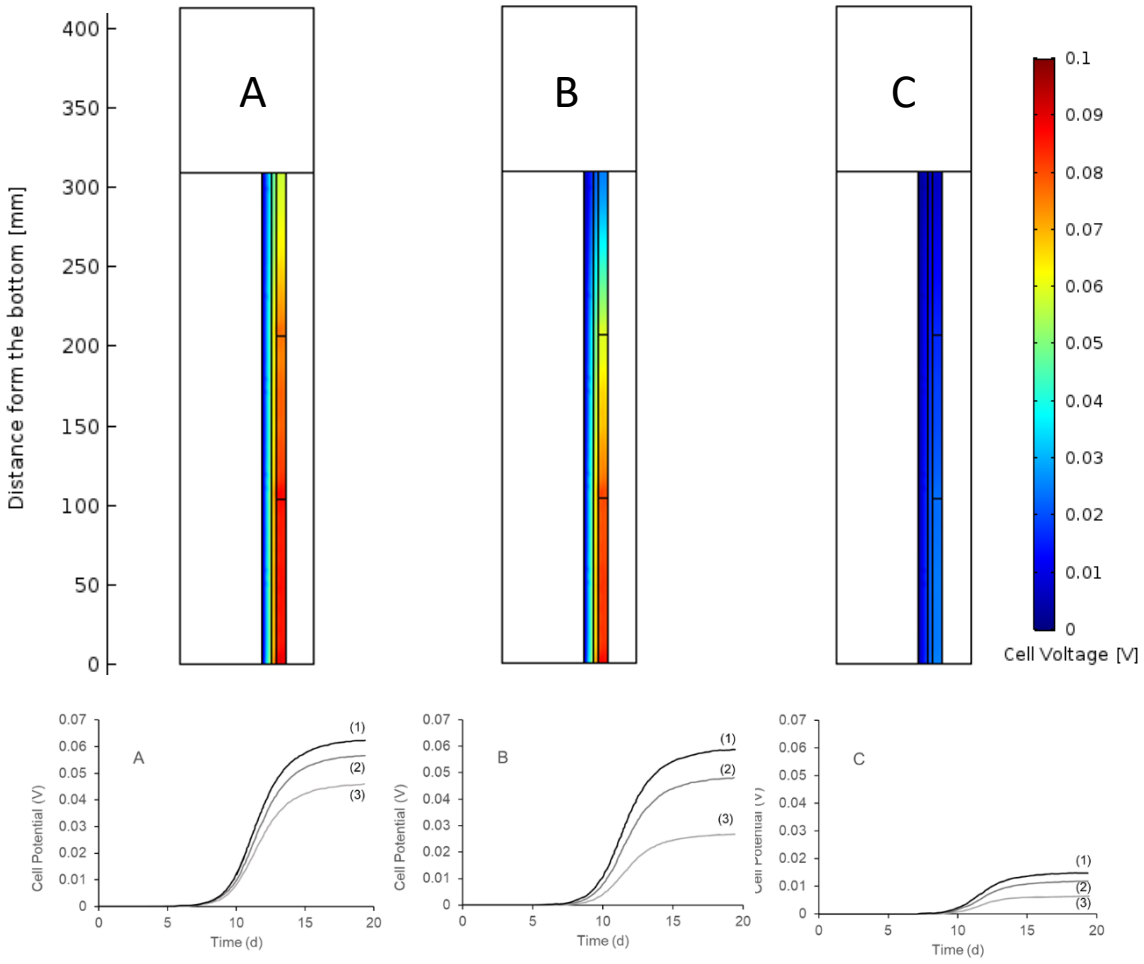

Figure 4. Output voltage generated by the SMFCs as predicted by the model for different soils and at different temperatures. Top: space profiles after 20 days. Bottom: trends with time. A) D_W = 6 cm^2 min^{-1} and T = 25 °C. B) D_W = 6 cm^2 min^{-1} and T = 40 °C. C) D_W = 0.8 cm^2 min^{-1} and T = 25 °C. (1) $SMFC_B$, (2) $SMFC_M$, (3) $SMFC_T$

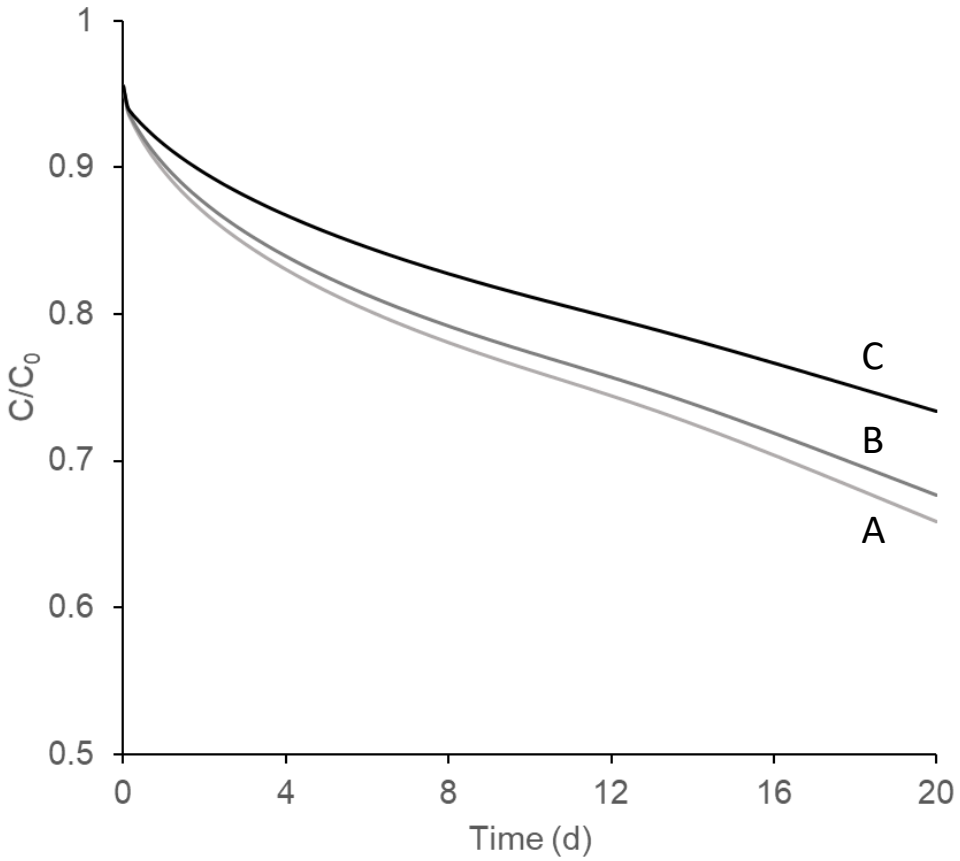

Figure 5. Concentration decay over time of hexachlorobenzene (concentration normalised to the initial value C_0) as predicted by the model for two types of soils and under two different temperatures. A) D_W = 6 cm^2 min^{-1} and T = 25 °C. B) D_W = 6 cm^2 min^{-1} and T = 40 °C. C) D_W = 0.8 cm^2 min^{-1} and T = 25 °C.

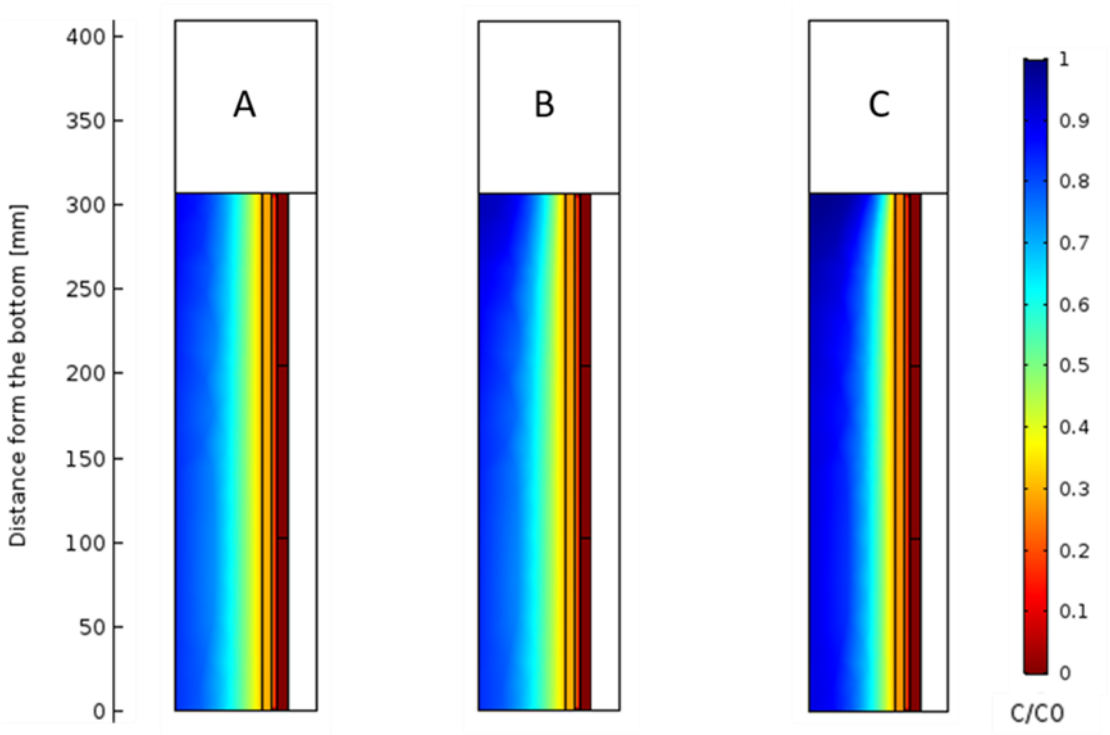

Figure 6. Space profiles of hexachlorobenzene concentration (normalised by the initial concentration C_0), after 20 days of treatment in the soil-MFC system. A) D_W = 6 cm^2 min^{-1} and T = 25 °C. B) D_W = 6 cm^2 min^{-1} and T = 40 °C. C) D_W = 0.8 cm^2 min^{-1} and T = 25 °C

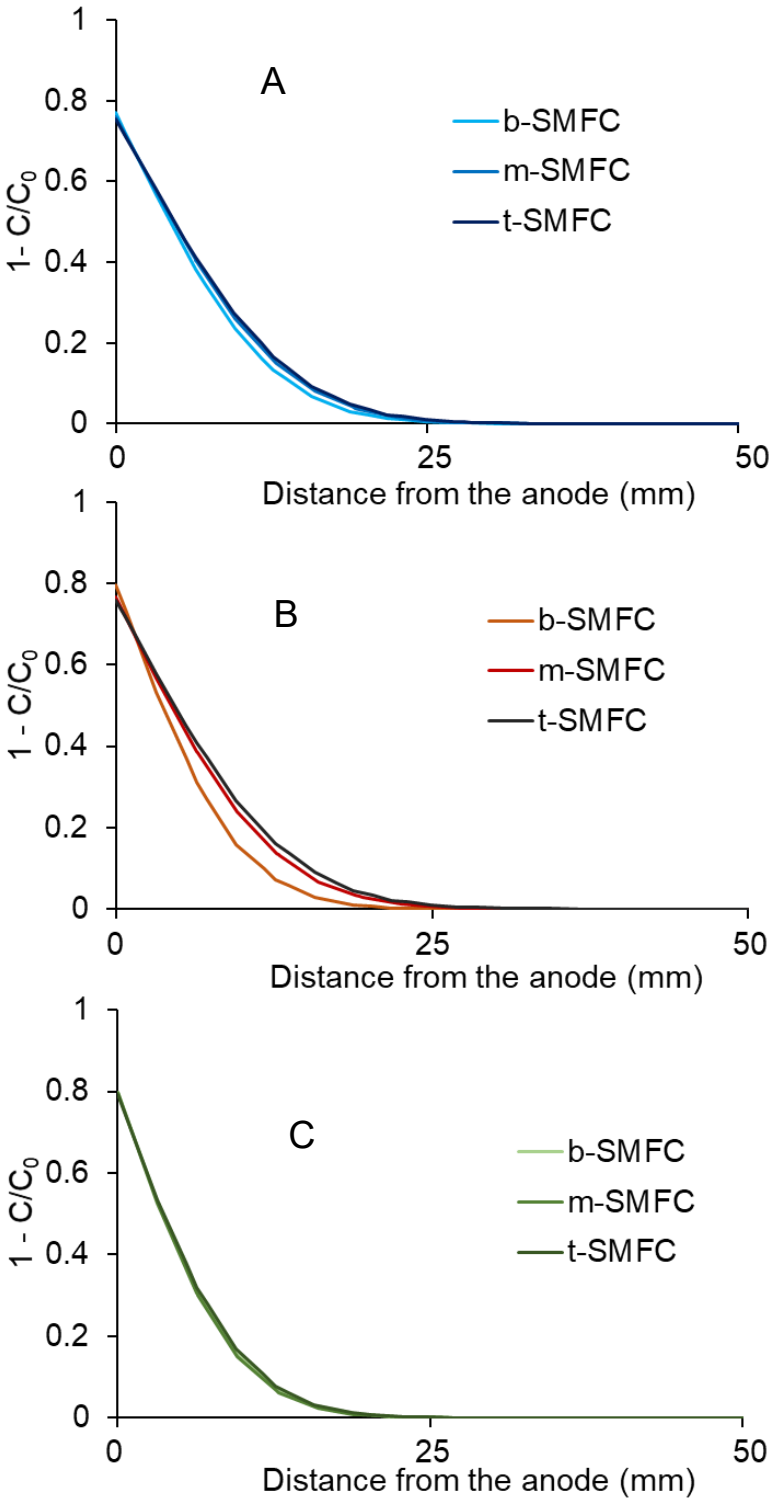

Figure 7. Space profiles of hexachlorobenzene concentration (normalised by the initial concentration C_0) from the central section of the fuel cells after 20 days of treatment in the soil-SMFC system A) D_W = 6 cm^2 min^{-1} and T = 25 °C. B) D_W = 6 cm^2 min^{-1} and T = 40 °C. C) D_W = 0.8 cm^2 min^{-1} and T = 25 °C